

Evidence of nested quasi-one-dimensional Fermi surface and decoupled charge-lattice orders in layered TaTe₂

Yi Lin ^{1,*} Maximillian Huber,¹ Sangeeta Rajpurohit,² Yanglin Zhu,⁴ Khalid M. Siddiqui,¹ Daniel H. Eilbott ³, Luca Moreschini,^{1,3} Ping Ai,¹ Jonathan D. Denlinger,⁵ Zhiqiang Mao,⁴ Liang Z. Tan ² and Alessandra Lanzara^{1,3,†}

¹Materials Sciences Division, Lawrence Berkeley National Laboratory, Berkeley, California 94720, USA

²Molecular Foundry, Lawrence Berkeley National Laboratory, Berkeley, California 94720, USA

³Department of Physics, University of California, Berkeley, California 94720, USA

⁴Department of Physics, The Pennsylvania State University, University Park, Pennsylvania 16802, USA

⁵Advanced Light Source, Lawrence Berkeley National Laboratory, Berkeley, California 94720, USA



(Received 7 December 2021; revised 15 March 2022; accepted 18 March 2022; published 13 April 2022)

The formations of charge and lattice orders are generally coupled in charge density wave (CDW) materials and share identical order wave vectors. Although this situation is usually satisfied in a large class of two-dimensional materials, it falls short in describing the so-called CDW-like phase transition in layered tantalum ditelluride (TaTe₂), accompanied by anomalous low temperature transport properties and a periodic lattice distortion (PLD). Here we combine angle-resolved photoemission spectroscopy and low energy electron diffraction to directly access the charge and lattice structures in 1T-polytypic TaTe₂ and study the anomalous phase transition. Our data reveal the presence of a surprising quasi-one-dimensional Fermi surface with nesting (FSN) condition, despite its van der Waals layered structure. We find that the wave vectors of the FSN and PLD are different, suggesting the decoupled formation between charge and lattice orders. These conditions are accompanied by rich footprints in band structure, including Fermi surface suppression, minigaps, and satellite bands. Our results suggest that TaTe₂ manifests intrinsic mixed dimensionality between its electronic and lattice structure and that the CDW-like phase transition is likely governed by multiple mechanisms. Our work provides routes for forging unconventional CDW phases and charge-lattice entanglement that would otherwise not be available in materials with fixed dimensionality.

DOI: [10.1103/PhysRevResearch.4.L022009](https://doi.org/10.1103/PhysRevResearch.4.L022009)

The study of charge density waves has been a topic of great interest over several decades both for basic science, being at the core of a variety of novel phenomena such as superconductivity [1–3], and for applications, given the easy tunability of charges [4–7].

The standard understanding of charge density wave (CDW) formation is based on the presence of a strong entanglement between charge and lattice [8–10]. The idea suggests that, in some metallic systems, below a certain temperature, parts of their electronic structure are nested by a characteristic wave vector, realizing a condition known as Fermi surface nesting (FSN). This nesting leads to periodic modulations of the charge with a consequent reorganization of its ionic potential and the formation of periodic lattice distortions (PLD). Under these conditions, the ground-state charge order is believed to be eventually commensurate with the underlying lattice order, and the FSN wave vector coincides with those of the PLD and CDW. In an ideal case, the CDW phase transition

is accompanied by a metal-insulator transition with a global band gap opening.

While this model has been generally accepted for explaining the CDW phase transition in one-dimensional (1D) and quasi-1D limits [11–16], our knowledge of charge density waves and specifically of the charge-lattice entanglement remains somewhat limited, especially in higher dimensions [17,18]. Indeed, in a growing number of layered or three-dimensional materials, even if the periodic charge modulation is dominant, typical signatures of a CDW phase transition, such as FSN, peaks in Lindhard function, Kohn's anomaly and metal-insulator transition, are often missing [17–19].

TaTe₂, a layered transition metal dichalcogenide, represents a canonical example where the standard description of CDW phase transition does not hold, and the role and degree of charge-lattice entanglements at the phase transition remains elusive. In contrast to those in other members of the tantalum dichalcogenide family, such as the widely studied TaS₂ and TaSe₂ [20,21], the lattice distortion and transport properties of TaTe₂ appear to be abnormal. Earlier reports have shown a structural phase transition at temperature $T \sim 170$ K [22–28], manifesting a PLD detected by Raman spectroscopy [24], diffraction [28,29] and more recently visualized by scanning transmission electron microscopy (STEM) [26]. However, such a structural transition is characterized by a steplike decrease of the resistivity at the phase transition upon cooling [22,23,27,30,31], in contrast to the typical CDW transition

*yilin@lbl.gov

†ALanzara@lbl.gov

Published by the American Physical Society under the terms of the [Creative Commons Attribution 4.0 International](https://creativecommons.org/licenses/by/4.0/) license. Further distribution of this work must maintain attribution to the author(s) and the published article's title, journal citation, and DOI.

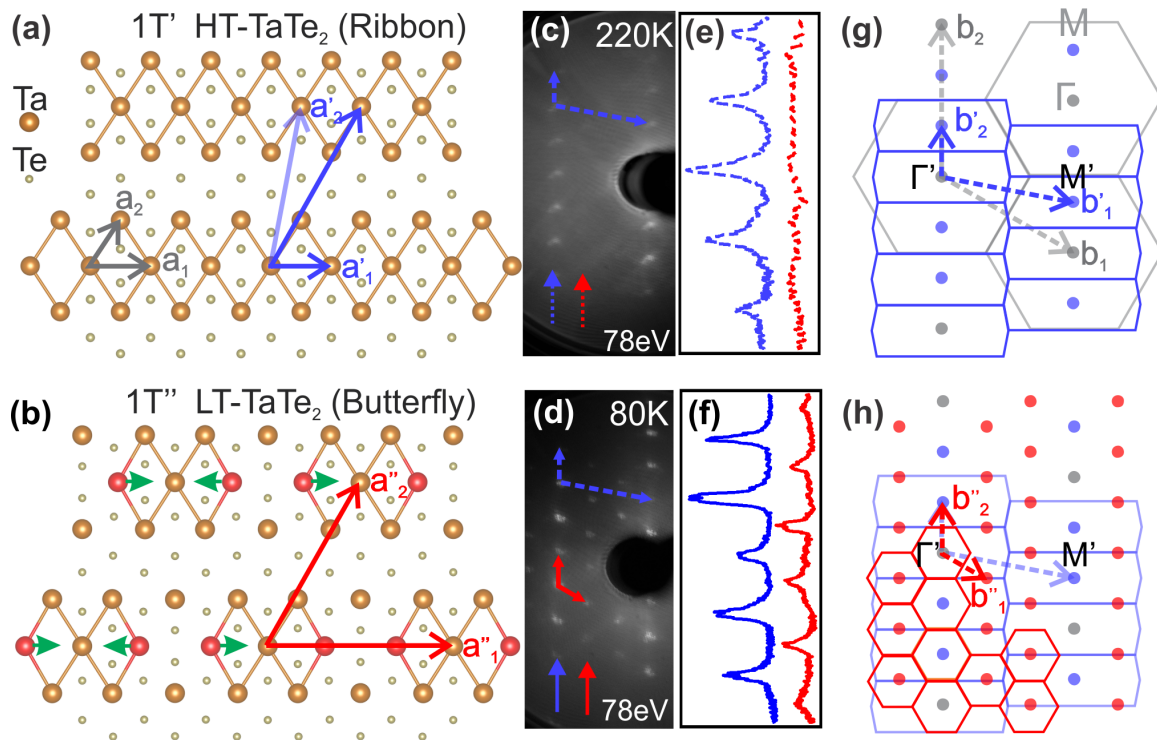


FIG. 1. Top view of (a) HT-TaTe₂ and (b) LT-TaTe₂ surface layer. Nominal 1T-TaTe₂ 1 × 1 primitive lattice vectors in gray; HT 3 × 1 primitive lattice vectors in blue (semitransparent blue vector shows an alternative choice); LT 3 × 3 primitive lattice vectors in pink. LEED pattern for (c) HT and (d) LT, with respective intensity profiles shown in (e,f). Reciprocal lattices for (g) HT and (h) LT. Reciprocal lattice vectors and Brillouin zones are labeled in gray, blue, and red for 1T-TaTe₂, HT-TaTe₂, and LT-TaTe₂, respectively.

behavior, where a steplike increase is usually expected [17]. Because of this apparent discrepancy and the difficulty of theoretical models to address this resistance anomaly [22–24,32–36], a term “CDW-like” has been minted to account for the phase transition in TaTe₂ [24,25,28,33].

Insights on how this CDW-like phase transition emerges can come from a detailed energy- and momentum-resolved study of the material band structure. To date, few reports exist in the literature [37,38], leaving our understanding of the physics of 1T-polytypic TaTe₂ incomplete. Previous ARPES results on 1T'-TaTe₂ suffered from the contamination of a “2H phase” on the surface [37]. Consequently, a threefold Fermi surface was found with no signatures of FSN, leading to an apparent disagreement with the anisotropy previously reported in structural and transport measurements for the 1T-polytypic TaTe₂ [27,30].

To resolve these controversies, we studied the crystal and electronic structures of 1T-polytypic TaTe₂ through a combination of low energy electron diffraction (LEED) and angle-resolved photoemission spectroscopy (ARPES). The details of sample preparation and instrumentation are provided in the Supplemental Material [39]. ARPES measurements reveal the band structure of 1T'-TaTe₂ across the phase transition. The band structure features a surprising quasi-1D Fermi surface at high temperature (HT), with a nearly perfect FSN condition whose nesting vector does not coincide with the PLD vector that develops at low temperature (LT). These results suggest a charge instability and a decoupled formation of charge and lattice orders throughout the phase transition and implies the possibility of incommen-

surability in the ground state. This incongruent situation is not seen in the CDW prototypes, where the FSN, PLD, and CDW share the same wave vector and ultimately favor a commensurate ground state [17,18].

In Fig. 1 we report LEED measurements on TaTe₂ surface and show their connection to the lattice structure in real and reciprocal space. Panels (a,b) present the top view of the crystal structure above and below the transition temperature (~170 K). At HT [panel (a)], TaTe₂ maintains a 1T' (distorted monoclinic) crystal structure [25,33,40,41], deformed from a nominal 1T (monoclinic) structure [22,32,35,42,43]. The Ta atoms form in-plane ribbon (double-zigzag) chains with a 3 × 1 primitive cell (blue vectors), with respect to the 1 × 1 1T primitive cell (gray vectors). In contrast, at LT [panel (b)], the Ta atoms are horizontally displaced (trimerized) as shown by the green arrows, forming a 1T'' structure. The distortion breaks the Ta ribbon chain into butterflylike clusters and leads to an extended 3 × 3 supercell indicated by the red vectors. The corresponding LEED patterns for our sample at HT and LT are shown in panels (c,d), respectively. The relative intensity profiles for the primary and the satellite LEED patterns are shown in panels (e,f). At HT [panels (c,e)], only the primary diffraction peaks (blue vectors) are present, supporting the existence of the 3 × 1 primitive cell. In contrast, at LT, beside the primary peaks, additional satellite peaks appear [see red vector and intensity profile in panels (d,f)], demonstrating the onset of a PLD forming the extended 3 × 3 supercell. In panels (g,h), we show the Brillouin zones and reciprocal lattice vectors at HT and LT, corresponding to the 3 × 1 and 3 × 3 unit cells described earlier. From the recip-

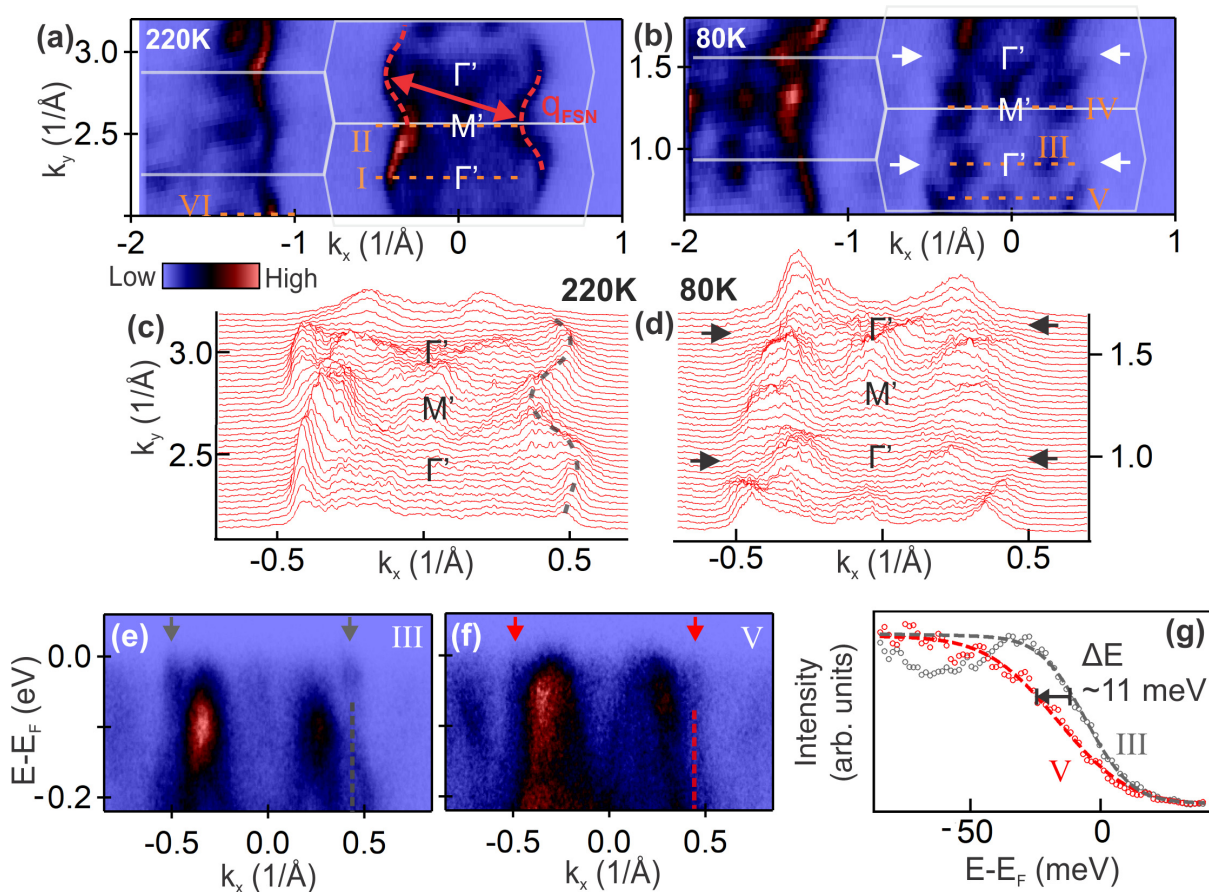


FIG. 2. Fermi surface of (a) HT-TaTe₂ and (b) LT-TaTe₂. The red vector in (a) denotes the FSN wave vector. Momentum distribution curves (MDCs) extracted at the Fermi surface for (c) HT and (d) LT. Horizontal arrows in (b,d) indicate the intensity suppressions in the nested Fermi contours. (e,f) Dispersions from cuts III and V in (b). (g) EDCs extracted at the momenta indicated by the vertical dashed lines in (e,f).

rocal lattice and the data, we extract the wave vector of the PLD [red vector b_1'' in panel (h)] with a magnitude of 0.66 \AA^{-1} based on the structure in panel (b).

In Fig. 2 we present the TaTe₂ electronic structure measured by ARPES. Panels (a,b) present the Fermi surface maps at HT and LT. Despite the quasi-two-dimensional (2D) layered structure of TaTe₂, we find that its Fermi surface is quasi-1D and twofold, in contrast to the threefold symmetry previously reported [37,38]. At HT [panels (a,c)], the Fermi surface shows a pair of antiparallel quasi-1D wavy contours along the k_y direction around $k_x = \pm 0.5 \text{ \AA}^{-1}$, pointing to the presence of highly anisotropic coupling between the in-plane axes. Even more interesting, we find that these wavy Fermi contours satisfy the Fermi surface nesting condition, as they can be perfectly translated on top of each other through a FSN vector equal to $\sim 0.85 \text{ \AA}^{-1}$, shown by the double-headed vector in panel (a). The observation of the FSN provides direct evidence of a charge instability in TaTe₂. Within these outer wavy Fermi surface contours, other features are present. However, none of them appears to be relevant for the FSN. In the LT data [panels (b,d)], we observe a suppression of the spectral weight in the region of the nested wavy Fermi surface sheets, as indicated by the horizontal arrows.

To better understand the spectral weight suppression along the nested Fermi surface and the energy gap that may be associated with it, we compare the evolution of the band

structure near the Fermi level between the gapped area (cut III) and metallic area (cut V) labeled in Fig. 2(b). Figures 2(e) and 2(f) show the corresponding dispersions, with the external bands constituting the wavy FS sheets indicated by the vertical arrows. Already from the band plots, one can see that while the external bands in panel (e) (indicated by the gray arrows) reach the Fermi level, the bands in panel (f) (indicated by the red arrows) do not, suggesting that the observed spectral weight suppression is likely due to the opening of local energy gaps. This is more evident in panel (g), where we compare the energy distribution curves (EDCs) corresponding to the momentum locations indicated by the gray and red dashed lines in panels (e,f). A clear energy downshift of the leading edge is observed for the red EDC from the gapped region with respect to the gray one from the metallic region. The overall magnitude of the energy shift (ΔE) is 11 meV, which estimates the size of the local gaps. The observation of the FSN and the appearance of the energy gaps suggest the presence of a charge-related symmetry breaking in the TaTe₂.

The band structure near high symmetry points is shown in Fig. 3. As a guide to the eye, along the red dashed lines in panels (a,c), near Γ' , the bands mainly display a double-hump shape. In contrast, near M' , the bands resemble the cross section of a cone, as illustrated by the red dashed lines in panels (b,d). These major band shapes are observed in both HT and LT, and therefore are robust towards the phase transition. We

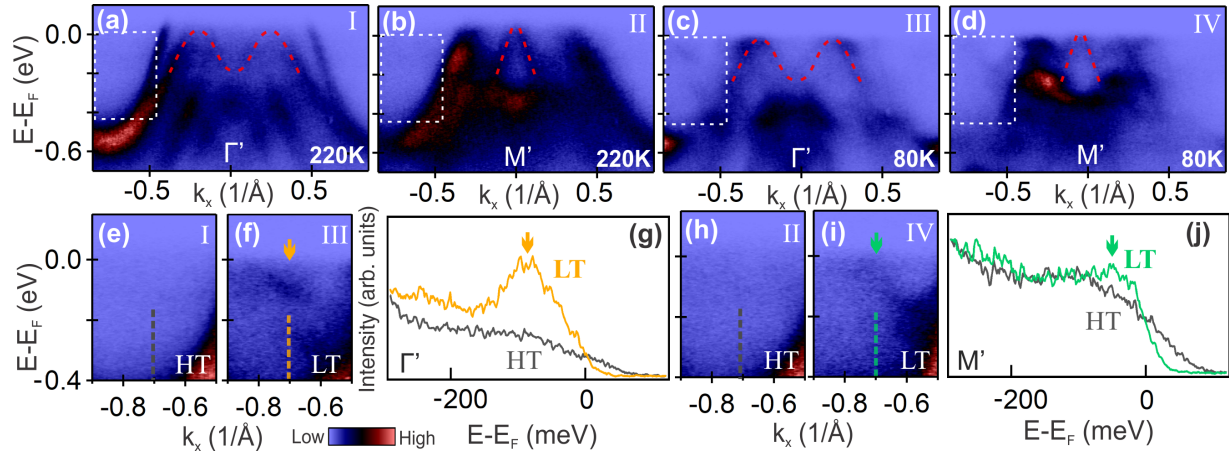


FIG. 3. Dispersions near high symmetry points. Panels (a–d) are extracted from cuts I–IV in Fig. 2. Panels (e,f) [(h,i)] present the zoomed-in views of the bands in the white dashed square areas in panels (a,c) [(b,d)], respectively. Panel (g) [panel (j)] presents the EDCs extracted at the momenta of the vertical dashed lines in panels (e,f) [panels (h,i)].

now focus on the interesting changes in the band structure, where we observe the appearance of satellite bands in the LT phase, in the white dashed square areas of Figs. 3(a)–3(d). We provide a closer look at these areas in panels (e–j), which reveal the appearance of new satellite bands in the LT phase, indicated by the arrows in panels (f,i). These satellite bands do not exist in panels (e,h) of HT. The contrast is further visible in the direct comparison between the raw EDCs shown in panel (g) [panel (j)], extracted from the momenta indicated by the dashed lines in panels (e,f) [panels (h,i)]. These satellite features are attributed to the band-folding effects induced by the periodic perturbations formed at the phase transition.

In Fig. 4 we report the formation of minigaps at higher binding energies. Panels (a–d) show the measured dispersions

near Γ' at different temperatures. At lower temperatures, a suppression of spectral weight is observed at binding energies around -0.1 and -0.27 eV, which manifest the minigap openings. The persistence of the suppression at a different photon energy [see panel (e)] rules out matrix element effects as a trivial origin. As the temperature increases, minigaps tend to fade [panels (a–c)] and eventually fully disappear above the transition temperature (>170 K) in panel (d). To understand the origin of the formation of these minigaps, we performed density functional theory (DFT) band calculations, based on the LT-TaTe₂ surface structure in Fig. 1(b) (see more computational details in the Supplemental Material [39]). When the 3×3 lattice superstructure is included for the PLD in the LT phase, the calculated spectral weight [panel (f)] reproduces

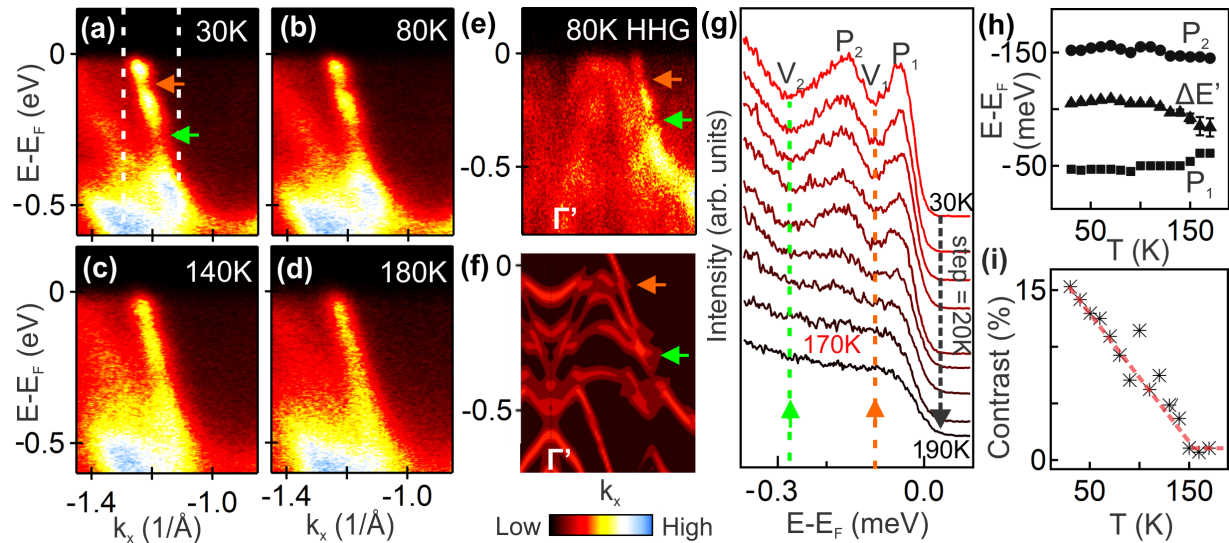


FIG. 4. Temperature-dependent measurements on minigaps. Dispersions near Γ' [at cut VI in Fig. 2(a)] with minigaps at (a) 30 K, (b) 80 K, (c) 140 K, and (d) 180 K. The orange and green arrows point to the minigaps. (e) Minigaps reproduced via a HHG ultrafast laser source at 21.3 eV. (f) Calculated spectral weights of LT-TaTe₂. (g) EDCs at different temperatures. P_1 , P_2 , V_1 , and V_2 label the intensity peaks and valleys (minigaps). (h) Temperature-dependent energy positions of P_1 and P_2 . The energy interval between P_1 and P_2 is defined as $\Delta E'$. (i) Intensity contrast between the peaks and valleys at different temperatures. Contrast = $[I(P) - I(V)] / [I(P) + I(V)]$, where $I(P) = I(P_1) + I(P_2)$, $I(V) = I(V_1) + I(V_2)$. $I(X)$ defines the intensity (I) at energy location X .

reasonably well the bands and the existence of the minigaps with the calculated positions around -0.1 and -0.3 eV. The agreement suggests that the minigaps are more likely the footprints of the PLD-induced superstructure than being directly linked to the charge instability induced by the FSN of the different wave vector.

These minigaps are further studied in Fig. 4(g), using the EDCs extracted from the momenta between the dashed lines in panel (a). The positions of the valleys (V_1 and V_2) in the spectra define the positions of the minigaps. The temperature dependence of the two peaks (P_1 and P_2) is shown in panel (h). The peak to peak energy difference ($\Delta E'$) is taken as an approximate size of the minigap V_1 , which remains largely constant around 110 meV at LT, with a slight decrease, up to 20–30 meV, in proximity of the transition temperature (above ~ 140 K). It is interesting to note that rather than a simple scenario of gap closing, the data instead suggest an additional but dominating scenario of gap filling. The gap filling is better measured by the intensity contrast between the valleys and peaks at different temperatures in panel (i). Different from the slightly changing gap size, the intensity contrast approximately shows a linear drop on raised temperature, eventually reaching zero above ~ 160 K, where the peaks and valleys can no longer be distinguished. A similar trend (filling of the minigaps at almost constant gap size) has been reported in prior studies for the quasi-1D CDW material NbSe₃ and has been attributed to the weakening of long-range interchain phase coherence, as opposed to the reduction of the order amplitude seen in conventional CDWs of Peierls origin [44,45].

In summary, the data presented so far show that the topology of the Fermi surface is dictated by the highly anisotropic twofold configuration. The quasi-1D wavy FS sheets committed FSN and local intensity suppression due to symmetry breakings. At the same time, a new lattice periodicity is caused by the PLD, whose fingerprints are present in the LT electronic structure as minigaps. However, the CDW-like material manifests two different wave vectors, one of the FSN ($q^{\text{FSN}} = 0.86 \text{ \AA}^{-1}$), and one corresponding to the PLD ($q^{\text{PLD}} = 0.66 \text{ \AA}^{-1}$). These wave vectors are incongruent, suggesting the decoupled formations of charge and lattice orders.

To account for these intriguing observations, we propose a scenario where the CDW-like phase transition in TaTe₂ is driven by multiple mechanisms due to mixed dimensionalities. Recently, effects of mixed dimensionality have also attracted great attention in investigating the possible multiple driving forces at the origin of complex CDW systems [18,44,46–49]. Conventionally, two mechanisms have been often discussed for explaining CDW formations: (i) Fermi surface nesting (pure charge instability), mostly preferred in 1D or quasi-1D systems [11–16], and (ii) q -dependent electron-phonon coupling, mostly responsible for CDW formation in 2D materials [18,38,50–53].

Our results suggest that TaTe₂ represents an interesting example of a material with mixed dimensionality, rooted in its unique combination of the nested quasi-1D Fermi surface within the overall 2D layered structure. This nested quasi-1D Fermi surface, often observed by ARPES in 1D or quasi-1D atom chains, is quite rare and in fact unreported in the Fermi surface measured from other layered tantalum or ditel-

luride families, TaX₂ ($X = \text{S, Se}$) [54,55] or ZTe₂ ($Z = \text{Nb, Ti, Ir, La, U}$) [38,56–60], despite the presence of a similar ribbon-chain-like lattice structure in some of them [38,61,62]. Overall, TaTe₂ electronic structure appears to be more 1D-like than those in prototypical 2D layered materials, while its crystal structure tends to be clearly more 2D-like than those of 1D chainlike systems.

This mixed dimensionality could lead to the CDW-like transition being governed by multiple mechanisms. On the one hand, several prior publications have argued that q -dependent electron-phonon coupling is the mechanism responsible for the phase transition in layered TaTe₂ [20,24,27,28,32,37,38,41,42], which could explain the PLD. On the other hand, our observed quasi-1D FSN and the local FS suppression suggest an additional mechanism at play, the charge instability of typical Peierls systems. While these two mechanisms usually occur separately in materials with fixed dimensionalities, here they seem to coexist independently, which results in the different PLD and FSN wave vectors. In addition, our observation of the gap-filling behavior of minigaps at higher temperatures suggests the long-range phase coherence within the LT TaTe₂ [44,45], which could further complicate the dimensionality effect via interchain or interlayer couplings.

Finally, we argue that our observation of the incommensurate FSN and PLD wave vectors provides a hint to understanding the intriguing anomalous resistivity drop observed in TaTe₂ [22,23,27,30]. Prior theoretical work [24,33] suggests a decrease of density of state near the Fermi level in LT-TaTe₂, which seems counterintuitive given the decrease in resistivity. Indeed, in conventional CDW phase transition, the electron density is believed to be ultimately locked in to the lattice modulation in a commensurate ground state. This scenario naturally leads to an increase of the resistivity at LT. In contrast, when the formations of charge and lattice order are decoupled, the incommensurate wave vector configuration could release part of the electrons at the Fermi level from the locked-in confinement to the lattice modulation, leading to an increased electron mobility and to a decrease of the resistivity, despite a lower number of charge carriers. To seek for more definitive explanation for the anomalous resistivity behavior in TaTe₂, finer ARPES inspections of the complicated multi-band structure near the Fermi surface and their variation in samples at different Te doping levels [30] are of strong interest for future work.

ACKNOWLEDGMENTS

This work was primarily supported by the U.S. Department of Energy (DOE), Office of Science, Office of Basic Energy Sciences, Materials Sciences and Engineering Division under Contract No. DE-AC02-05CH11231 (Ultrafast Materials Science Program No. KC2203). This research used resources of the Advanced Light Source, a U.S. DOE Office of Science User Facility under Contract No. DE-AC02-05CH11231. Support for crystal growth and characterization was provided by the National Science Foundation through the Penn State 2D Crystal Consortium–Materials Innovation Platform (2DCC-MIP) under NSF Cooperative Agreement No. DMR-1539916. Theoretical efforts were primarily supported by

the Computational Materials Sciences Program funded by the U.S. Department of Energy, Office of Science, Basic Energy Sciences, Materials Sciences and Engineering Division. Additional support for ARPES intensity simulations

was provided through the Molecular Foundry, a DOE Office of Science User Facility supported by the Office of Science of the U.S. Department of Energy under Contract No. DE-AC02-05CH11231.

- [1] E. H. da Silva Neto, P. Aynajian, A. Frano, R. Comin, E. Schierle, E. Weschke, A. Gyenis, J. Wen, J. Schneeloch, Z. Xu, S. Ono, G. Gu, M. Le Tacon, and A. Yazdani, Ubiquitous Interplay Between Charge Ordering and High-Temperature Superconductivity in Cuprates, *Science* **343**, 393 (2014).
- [2] J. Chang, E. Blackburn, A. T. Holmes, N. B. Christensen, J. Larsen, J. Mesot, R. Liang, D. A. Bonn, W. N. Hardy, A. Watenphul, M. v. Zimmermann, E. M. Forgan, and S. M. Hayden, Direct observation of competition between superconductivity and charge density wave order in $\text{YBa}_2\text{Cu}_3\text{O}_{6.67}$, *Nat. Phys.* **8**, 871 (2012).
- [3] W. D. Wise, M. C. Boyer, K. Chatterjee, T. Kondo, T. Takeuchi, H. Ikuta, Y. Wang, and E. W. Hudson, Charge-density-wave origin of cuprate checkerboard visualized by scanning tunnelling microscopy, *Nat. Phys.* **4**, 696 (2008).
- [4] R. Comin, A. Frano, M. M. Yee, Y. Yoshida, H. Eisaki, E. Schierle, E. Weschke, R. Sutarto, F. He, A. Soumyanarayanan, Y. He, M. Le Tacon, I. S. Elfimov, J. E. Hoffman, G. A. Sawatzky, B. Keimer, and A. Damascelli, Charge Order Driven by Fermi-Arc Instability in $\text{Bi}_2\text{Sr}_{2-x}\text{La}_x\text{CuO}_6$, *Science* **343**, 390 (2014).
- [5] E. H. da Silva Neto, B. Yu, M. Minola, R. Sutarto, E. Schierle, F. Boschini, M. Zonno, M. Bluschke, J. Higgins, Y. Li, G. Yu, E. Weschke, F. He, M. Le Tacon, R. L. Greene, M. Greven, G. A. Sawatzky, B. Keimer, and A. Damascelli, Doping-dependent charge order correlations in electron-doped cuprates, *Sci. Adv.* **2**, e1600782 (2016).
- [6] B. Sipoš, A. F. Kusmartseva, A. Akrap, H. Berger, L. Forro, and E. Tutis, From Mott state to superconductivity in 1T-TaS_2 , *Nat. Mater.* **7**, 960 (2008).
- [7] T. Wu, H. Mayaffre, S. Kramer, M. Horvatic, C. Berthier, W. N. Hardy, R. Liang, D. A. Bonn, and M. H. Julien, Magnetic-field-induced charge-stripe order in the high-temperature superconductor $\text{YBa}_2\text{Cu}_3\text{O}_y$, *Nature (London)* **477**, 191 (2011).
- [8] R. E. Peierls, *Quantum Theory of Solids* (Clarendon Press, Oxford, UK, 1996).
- [9] H. Fröhlich, On the theory of superconductivity: the one-dimensional case, *Proc. R. Soc. London, Ser. A* **223**, 296 (1954).
- [10] G. Grüner, *Density Waves in Solids* (CRC Press, Boca Raton, FL, 2018).
- [11] F. Zwick, D. Jérôme, G. Margaritondo, M. Onellion, J. Voit, and M. Grioni, Band Mapping and Quasiparticle Suppression in the One-Dimensional Organic Conductor TTF-TCNQ, *Phys. Rev. Lett.* **81**, 2974 (1998).
- [12] M. Sing, U. Schwingenschlögl, R. Claessen, P. Blaha, J. M. P. Carmelo, L. M. Martelo, P. D. Sacramento, M. Dressel, and C. S. Jacobsen, Electronic structure of the quasi-one-dimensional organic conductor TTF-TCNQ, *Phys. Rev. B* **68**, 125111 (2003).
- [13] R. Claessen, M. Sing, U. Schwingenschlögl, P. Blaha, M. Dressel, and C. S. Jacobsen, Spectroscopic signatures of spin-charge separation in the quasi-one-dimensional organic conductor TTF-TCNQ, *Phys. Rev. Lett.* **88**, 096402 (2002).
- [14] J. N. Crain, A. Kirakosian, K. N. Altmann, C. Bromberger, S. C. Erwin, J. L. McChesney, J. L. Lin, and F. J. Himpsel, Fractional band filling in an atomic chain structure, *Phys. Rev. Lett.* **90**, 176805 (2003).
- [15] H. W. Yeom, S. Takeda, E. Rotenberg, I. Matsuda, K. Horikoshi, J. Schaefer, C. M. Lee, S. D. Kevan, T. Ohta, T. Nagao, and S. Hasegawa, Instability and Charge Density Wave of Metallic Quantum Chains on a Silicon Surface, *Phys. Rev. Lett.* **82**, 4898 (1999).
- [16] K. Yaji, I. Mochizuki, S. Kim, Y. Takeichi, A. Harasawa, Y. Ohtsubo, P. Le Fèvre, F. Bertran, A. Taleb-Ibrahimi, A. Kakizaki, and F. Komori, Fermi gas behavior of a one-dimensional metallic band of Pt-induced nanowires on Ge(001), *Phys. Rev. B* **87**, 241413(R) (2013).
- [17] X. Zhu, J. Guo, J. Zhang, and E. W. Plummer, Misconceptions associated with the origin of charge density waves, *Adv. Phys.: X* **2**, 622 (2017).
- [18] X. Zhu, Y. Cao, J. Zhang, E. W. Plummer, and J. Guo, Classification of charge density waves based on their nature, *Proc. Natl. Acad. Sci. USA* **112**, 2367 (2015).
- [19] P. Monceau, Electronic crystals: an experimental overview, *Adv. Phys.* **61**, 325 (2012).
- [20] J. A. Wilson, F. J. Di Salvo, and S. Mahajan, Charge-Density Waves in Metallic, Layered, Transition-Metal Dichalcogenides, *Phys. Rev. Lett.* **32**, 882 (1974).
- [21] J. A. Wilson, F. J. Di Salvo, and S. Mahajan, Charge-density waves and superlattices in the metallic layered transition metal dichalcogenides, *Adv. Phys.* **24**, 117 (1975).
- [22] T. Sörgel, J. Nuss, U. Wedig, R. K. Kremer, and M. Jansen, A new low temperature modification of TaTe_2 —Comparison to the room temperature and the hypothetical 1T-TaTe_2 modification, *Mater. Res. Bull.* **41**, 987 (2006).
- [23] A. Vernes, H. Ebert, W. Bensch, W. Heid, and C. Näther, Crystal structure, electrical properties and electronic band structure of tantalum ditelluride, *J. Phys.: Condens. Matter* **10**, 761 (1998).
- [24] J. J. Gao, J. G. Si, X. Luo, J. Yan, F. C. Chen, G. T. Lin, L. Hu, R. R. Zhang, P. Tong, W. H. Song, X. B. Zhu, W. J. Lu, and Y. P. Sun, Origin of the structural phase transition in single-crystal TaTe_2 , *Phys. Rev. B* **98**, 224104 (2018).
- [25] J. Feng, A. Tan, S. Wagner, J. Liu, Z. Mao, X. Ke, and P. Zhang, Charge modulation and structural transformation in TaTe_2 studied by scanning tunneling microscopy/spectroscopy, *Appl. Phys. Lett.* **109**, 021901 (2016).
- [26] I. El Baggari, N. Sivadas, G. M. Stiehl, J. Waelder, D. C. Ralph, C. J. Fennie, and L. F. Kourkoutis, Direct Visualization of Trimerized States in $1\text{T}'\text{-TaTe}_2$, *Phys. Rev. Lett.* **125**, 165302 (2020).
- [27] H. Chen, Z. Li, L. Guo, and X. Chen, Anisotropic magneto-transport and magnetic properties of low-temperature phase of TaTe_2 , *EPL* **117**, 27009 (2017).

- [28] K. M. Siddiqui, D. B. Durham, F. Cropp, C. Ophus, S. Rajpurohit, Y. Zhu, J. D. Carlström, C. Stavrakas, Z. Mao, A. Raja, P. Musumeci, L. Z. Tan, A. M. Minor, D. Filippetto, and R. A. Kaindl, Ultrafast optical melting of trimer superstructure in layered 1T'-TaTe₂, *Commun. Phys.* **4**, 152 (2021).
- [29] V. Petkov, K. Chapagain, J. Yang, S. Shastri, and Y. Ren, Bonding interactions and coexistence of chemically distinct periodic lattice distortions in the charge density wave compound TaTe₂, *Phys. Rev. B* **102**, 024111 (2020).
- [30] Y.-C. Luo, Y.-Y. Lv, R.-M. Zhang, L. Xu, Z.-A. Zhu, S.-H. Yao, J. Zhou, X.-X. Xi, Y. B. Chen, and Y.-F. Chen, Subtle effect of doping on the charge density wave in TaTe₂- δ ($\delta = 0.0280.123$) crystals revealed by anisotropic transport measurements and Raman spectroscopy, *Phys. Rev. B* **103**, 064103 (2021).
- [31] T. C. Hu, Q. Wu, Z. X. Wang, L. Y. Shi, Q. M. Liu, L. Yue, S. J. Zhang, R. S. Li, X. Y. Zhou, S. X. Xu, D. Wu, T. Dong, and N. L. Wang, Optical spectroscopy and ultrafast pump-probe study of the structural phase transition in 1T'-TaTe₂, *Phys. Rev. B* **105**, 075113 (2022).
- [32] Y. Liu, D. F. Shao, L. J. Li, W. J. Lu, X. D. Zhu, P. Tong, R. C. Xiao, L. S. Ling, C. Y. Xi, L. Pi, H. F. Tian, H. X. Yang, J. Q. Li, W. H. Song, X. B. Zhu, and Y. P. Sun, Nature of charge density waves and superconductivity in 1T-TaSe₂-xTex, *Phys. Rev. B* **94**, 045131 (2016).
- [33] C. Chen, H.-S. Kim, A. S. Admasu, S.-W. Cheong, K. Haule, D. Vanderbilt, and W. Wu, Trimer bonding states on the surface of the transition-metal dichalcogenide TaTe₂, *Phys. Rev. B* **98**, 195423 (2018).
- [34] M. H. Whangbo and E. Canadell, Analogies between the concepts of molecular chemistry and solid-state physics concerning structural instabilities. Electronic origin of the structural modulations in layered transition metal dichalcogenides, *J. Am. Chem. Soc.* **114**, 9587 (2002).
- [35] M.-L. Doublet, S. Remy, and F. Lemoigno, Density functional theory analysis of the local chemical bonds in the periodic tantalum dichalcogenides TaX₂ (X = S, Se, Te), *J. Chem. Phys.* **113**, 5879 (2000).
- [36] E. Canadell, S. P. Jobic, R. Brec, J. Rouxel, and M.-H. Whangbo, Importance of short interlayer Te...Te contacts for the structural distortions and physical properties of CdI₂-type layered transition-metal ditellurides, *J. Solid State Chem.* **99**, 189 (1992).
- [37] I. Kar, K. Dolui, L. Harnagea, Y. Kushnirenko, G. Shipunov, N. C. Plumb, M. Shi, B. Büchner, and S. Thirupathiah, Experimental Evidence of a Stable 2H Phase on the Surface of Layered 1T'-TaTe₂, *J. Phys. Chem. C* **125**, 1150 (2021).
- [38] C. Battaglia, H. Cercellier, F. Clerc, L. Despont, M. G. Garnier, C. Koitzsch, P. Aebi, H. Berger, L. Forró, and C. Ambrosch-Draxl, Fermi-surface-induced lattice distortion in NbTe₂, *Phys. Rev. B* **72**, 195114 (2005).
- [39] See Supplemental Material at <http://link.aps.org/supplemental/10.1103/PhysRevResearch.4.L022009> for details of sample growth, experimental settings, and computational methods.
- [40] H. Wang, K. Chai, L. Wei, Z.-A. Li, C. Zhu, D. Zheng, Z. Li, J. Li, H. Tian, H. Yang, and J. Li, Charge density wave and atomic trimerization in layered transition-metal dichalcogenides 1T-MX₂ materials, *EPL* **130**, 47001 (2020).
- [41] L.-L. Wei, S.-S. Sun, K. Sun, Y. Liu, D.-F. Shao, W.-J. Lu, Y.-P. Sun, H.-F. Tian, and H.-X. Yang, Charge Density Wave States and Structural Transition in Layered Chalcogenide TaSe₂-xTex, *Chin. Phys. Lett.* **34**, 086101 (2017).
- [42] S. Sharma, L. Nordström, and B. Johansson, Stabilization of charge-density waves in 1T-TaX₂ (X = S, Se, Te): First-principles total energy calculations, *Phys. Rev. B* **66**, 195101 (2002).
- [43] F. Lemoigno, M. L. Doublet, and S. Remy, Why has 1T-TaTe₂ not yet been synthesized? A DFT contribution, *Synth. Met.* **103**, 2679 (1999).
- [44] C. W. Nicholson, E. F. Schwier, K. Shimada, H. Berger, M. Hoesch, C. Berthod, and C. Monney, Role of a higher-dimensional interaction in stabilizing charge density waves in quasi-one-dimensional NbSe₃ revealed by angle-resolved photoemission spectroscopy, *Phys. Rev. B* **101**, 045412 (2020).
- [45] C. W. Nicholson, C. Berthod, M. Puppini, H. Berger, M. Wolf, M. Hoesch, and C. Monney, Dimensional Crossover in a Charge Density Wave Material Probed by Angle-Resolved Photoemission Spectroscopy, *Phys. Rev. Lett.* **118**, 206401 (2017).
- [46] D. Lin, S. Li, J. Wen, H. Berger, L. Forro, H. Zhou, S. Jia, T. Taniguchi, K. Watanabe, X. Xi, and M. S. Bahramy, Patterns and driving forces of dimensionality-dependent charge density waves in 2H-type transition metal dichalcogenides, *Nat. Commun.* **11**, 2406 (2020).
- [47] K. Rossnagel, On the origin of charge-density waves in select layered transition-metal dichalcogenides, *J. Phys.: Condens. Matter* **23**, 213001 (2011).
- [48] M. Calandra, I. I. Mazin, and F. Mauri, Effect of dimensionality on the charge-density wave in few-layer 2H-NbSe₂, *Phys. Rev. B* **80**, 241108(R) (2009).
- [49] K. Zhang, X. Liu, H. Zhang, K. Deng, M. Yan, W. Yao, M. Zheng, E. F. Schwier, K. Shimada, J. D. Denlinger, Y. Wu, W. Duan, and S. Zhou, Evidence for a Quasi-One-Dimensional Charge Density Wave in CuTe by Angle-Resolved Photoemission Spectroscopy, *Phys. Rev. Lett.* **121**, 206402 (2018).
- [50] J. M. Carpinelli, H. H. Weitering, E. W. Plummer, and R. Stumpf, Direct observation of a surface charge density wave, *Nature (London)* **381**, 398 (1996).
- [51] F. Clerc, C. Battaglia, H. Cercellier, C. Monney, H. Berger, L. Despont, M. G. Garnier, and P. Aebi, Fermi surface of layered compounds and bulk charge density wave systems, *J. Phys.: Condens. Matter* **19**, 355002 (2007).
- [52] M. D. Johannes and I. I. Mazin, Fermi surface nesting and the origin of charge density waves in metals, *Phys. Rev. B* **77**, 165135 (2008).
- [53] X. Xi, L. Zhao, Z. Wang, H. Berger, L. Forro, J. Shan, and K. F. Mak, Strongly enhanced charge-density-wave order in monolayer NbSe₂, *Nat. Nanotechnol.* **10**, 765 (2015).
- [54] T. Pillo, J. Hayoz, H. Berger, M. Grioni, L. Schlapbach, and P. Aebi, Remnant Fermi Surface in the Presence of an Underlying Instability in Layered TaS₂, *Phys. Rev. Lett.* **83**, 3494 (1999).
- [55] M. Bovet, D. Popović, F. Clerc, C. Koitzsch, U. Probst, E. Bucher, H. Berger, D. Naumović, and P. Aebi, Pseudogapped Fermi surfaces of 1T-TaS₂ and 1T-TaSe₂: A charge density wave effect, *Phys. Rev. B* **69**, 125117 (2004).
- [56] T. Straub, R. Claessen, P. Steiner, S. Hüfner, V. Eyert, K. Friemelt, and E. Bucher, Many-body definition of a Fermi surface: Application to angle-resolved photoemission, *Phys. Rev. B* **55**, 13473 (1997).
- [57] K. Kim, S. Kim, K. T. Ko, H. Lee, J. H. Park, J. J. Yang, S. W. Cheong, and B. I. Min, Origin of first-order-type electronic

- and structural transitions in IrTe₂, [Phys. Rev. Lett. **114**, 136401 \(2015\)](#).
- [58] D. Ootsuki, S. Pyon, K. Kudo, M. Nohara, M. Horio, T. Yoshida, A. Fujimori, M. Arita, H. Anzai, H. Namatame, M. Taniguchi, N. L. Saini, T. Mizokawa *et al.*, Electronic Structure Reconstruction by Orbital Symmetry Breaking in IrTe₂, [J. Phys. Soc. Jpn. **82**, 093704 \(2013\)](#).
- [59] D. R. Garcia, G. H. Gweon, S. Y. Zhou, J. Graf, C. M. Jozwiak, M. H. Jung, Y. S. Kwon, and A. Lanzara, Revealing charge density wave formation in the LaTe₂ system by angle resolved photoemission spectroscopy, [Phys. Rev. Lett. **98**, 166403 \(2007\)](#).
- [60] L. Miao, S. Liu, Y. Xu, E. C. Kotta, C.-J. Kang, S. Ran, J. Paglione, G. Kotliar, N. P. Butch, J. D. Denlinger, and L. A. Wray, Low Energy Band Structure and Symmetries of UTe₂ from Angle-Resolved Photoemission Spectroscopy, [Phys. Rev. Lett. **124**, 076401 \(2020\)](#).
- [61] M. Rumo, C. W. Nicholson, A. Pulkkinen, B. Hildebrand, G. Kremer, B. Salzmann, M.-L. Mottas, K. Y. Ma, E. L. Wong, M. K. L. Man, K. M. Dani, B. Barbiellini, M. Muntwiler, T. Jaouen, F. O. von Rohr, and C. Monney, Examining the surface phase diagram of IrTe₂ with photoemission, [Phys. Rev. B **101**, 235120 \(2020\)](#).
- [62] K. T. Ko, H. H. Lee, D. H. Kim, J. J. Yang, S. W. Cheong, M. J. Eom, J. S. Kim, R. Gammag, K. S. Kim, H. S. Kim, T. H. Kim, H. W. Yeom, T. Y. Koo, H. D. Kim, J. H. Park *et al.*, Charge-ordering cascade with spin-orbit Mott dimer states in metallic iridium ditelluride, [Nat. Commun. **6**, 7342 \(2015\)](#).